Third order polynomial bundle adjustment for optical calibration refinement.

Pietro Sperotto[1], Bo Watz[1], David Hess[1].

[1] Dantec Dynamics A/S, Copenaghen, Denmark.

*Corresponding author: pietro.sperotto@dantecdynamics.com

Keywords:

ABSTRACT

We propose a refinement and validity region expansion process of a 3rd order polynomial calibration based on bundle adjustment. The present methodology can be expanded to any model as long as the mapping is a smooth function. Both methods are tested with a tomographic Particle Tracking Velocimetry measurement whose results are compared in terms of the smoothness and length of the retrieved tracks. The refinement method shows a significant improvement in both the associated PDFs. Similarly, the expansion shows a corresponding behaviour to the original calibration even though a higher degree of smoothness of the tracks is achieved.

1. Introduction

Volumetric imaging velocimetry techniques requires precise camera calibrations to achieve a satisfactory reconstruction of the velocity field, especially for high seeding density. The calibration is crucial for both 3D Particle Image Velocimetry (PIV) (Elsinga et al., 2006) and Particle Tracking Velocimetry (PTV)(Maas et al., 1993). Two models are the most widespread in the PIV community: the third-order polynomial calibration, also referred to as Soloff model (Soloff et al., 1997), or a more classic pin-hole calibration. There are some pros and cons of each of these models, for instance, pin-hole calibration images do not require a traversing system. This is an advantage as the position on the calibration plate can be erroneous and further errors can be introduced. For instance, if the normal direction to the calibration plate and the displacement of the traversing system are not parallel. Furthermore, the pinhole calibration represents a physical model that reduces problems such as over-fitting. In contrast, the third-order polynomial is merely a mathematical approach and is more inclined to over-fit outliers in the calibration procedure. However, due to this flexible definition, the Soloff model can easily account for different mediums and better deal with interfaces such as glass walls. Differently, the pinhole calibration requires a physical model tweaking (Maas, 1996) depending on the mediums and the thicknesses of the various interfaces

that must be known, some of these parameters can be evaluated in situ Wieneke (2004). Another drawback of the third-order polynomial is that the calibration is valid only in the region where the dots or checker marks of the calibration plate are detected. This could be a problem for wide-angle setups and large-scale experiments. Indeed, in the former case, it is possible that the marks or dots are not properly detected due to steep angles, leading to a non-calibrated area or volume. In the latter case, the complexity is derived from the size of the measurement volume, to retrieve a satisfactory calibration, the plate should cover completely X, Y and Z. However, if an experiment is performed in a measurement volume of several $[m^3]$, it becomes exceedingly difficult to find a plate and traversing system to meet this criterion.

Further errors can be introduced in the time passing between the calibration and the measurements. The calibration can suffer from camera displacements, optical changes or medium changes. The most common type of error is generated by setup movement while removing the calibration plate after the acquisition of the calibration images, or vibration in the camera set-up. Many methods have been proposed to correct this change a posteriori by using low seeding density particle images, usually not exceeding 0.005 particles per pixel (ppp). The most known method is the self-calibration proposed by Wieneke (Wieneke, 2008). Nonetheless, other methods have been proposed by Cornic et al. (2015) and the Volumetric Calibration Refinement (VCR) by Bruecker et al. (2020), the latter would be used as the main comparison throughout this work.

2. Methodology

The method is based on the third order polynomial model assuming a generic position in the 3D space $\boldsymbol{X} = (X, Y, Z)$, then its projection $\boldsymbol{x}^i = \left(x^i, y^i\right)$ on the i^{th} camera is mapped by the following set of equations:

$$\begin{cases} x^i \simeq & F_x^i\left(\boldsymbol{X}\right) = a_{x0}^i + a_{x1}^i X + a_{x2}^i Y + a_{x3}^i Z + a_{x4}^i X^2 + a_{x5}^i XY + a_{x6}^i Y^2 + a_{x7}^i XZ \\ & + a_{x8}^i YZ + a_{x9}^i Z^2 + a_{x10}^i X^3 + a_{x11}^i X^2 Y + a_{x12}^i XY^2 + a_{x13}^i Y^3 \\ & + a_{x14}^i X^2 Z + a_{x15}^i XYZ + a_{x16}^i Y^2 Z + a_{x17}^i XZ^2 + a_{x18}^i YZ^2 \\ y^i \simeq & F_y^i\left(\boldsymbol{X}\right) = a_{y0}^i + a_{y1}^i X + a_{y2}^i Y + a_{y3}^i Z + a_{y4}^i X^2 + a_{y5}^i XY + a_{y6}^i Y^2 + a_{y7}^i XZ \\ & + a_{y8}^i YZ + a_{y9}^i Z^2 + a_{y10}^i X^3 + a_{y11}^i X^2 Y + a_{y12}^i XY^2 + a_{y13}^i Y^3 \\ & + a_{y14}^i X^2 Z + a_{y15}^i XYZ + a_{y16}^i Y^2 Z + a_{y17}^i XZ^2 + a_{y18}^i YZ^2 \end{cases} \tag{1}$$

The main objective of a bundle adjustment is to reduce the disparity error, defined as the error between the re-projected particle position and the sensor position:

$$J = \sum_{i=0}^{n_c-1} \sum_{k=0}^{n-1} \left(\left\| x_k^i - F_x^i\left(\boldsymbol{X}_k\right) \right\|_2^2 + \left\| y_k^i - F_y^i\left(\boldsymbol{X}_k\right) \right\|_2^2 \right), \tag{2}$$

where n is the number of particles and n_c is the number of cameras. It is important to distinguish two cases: position refinement and Bundle Adjustment (BA). Position refinement adjusts the particle position for a given calibration and any particle can be optimized independently, this process is equivalent to optimising the following:

$$\min_{\boldsymbol{X}_k} J_k = \sum_{i=0}^{n_c-1} \left(\left\| x_k^i - F_x^i\left(\boldsymbol{X}_k\right) \right\|_2^2 + \left\| y_k^i - F_y^i\left(\boldsymbol{X}_k\right) \right\|_2^2 \right). \tag{3}$$

In addition to improve the particle positions, BA also optimizes the camera's parameter $\boldsymbol{A}_{\cdot}^i = \left(a_{\cdot 0}^i, \ldots, a_{\cdot j}^i, \ldots, a_{\cdot 18}^i\right) \in \mathbb{R}^{19}$, where $< \cdot >$ represent x or y. Thus, BA can be used to improve previously computed calibrations. The only requirement is that all the particles must be optimized together:

$$\min_{\boldsymbol{X}_k, \boldsymbol{A}_x^i, \boldsymbol{A}_y^i} J = \sum_{i=0}^{n_c-1} \sum_{k=0}^{n-1} \left(\left\| x_k^i - F_x^i\left(\boldsymbol{X}_k\right) \right\|_2^2 + \left\| y_k^i - F_y^i\left(\boldsymbol{X}_k\right) \right\|_2^2 \right). \tag{4}$$

The computational costs between the two is sensibly different especially when a lot of particles are used in the optimization process.

In literature, it is often suggested (Triggs et al., 2000) to use a Cauchy distribution of errors for the BA to mitigate the effect of the outliers. However, this usually means a less robust optimization process. Nevertheless, the main interest for us is the new calibration rather than the particle positions, therefore, we prefer to remove outliers before the BA routine.

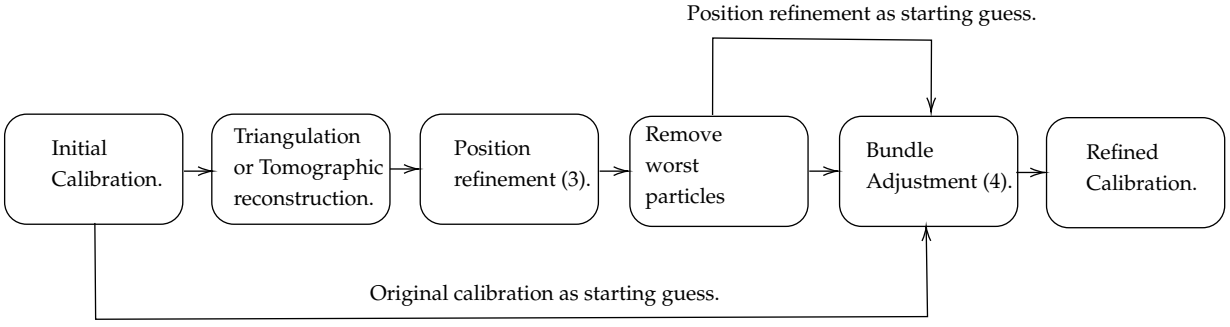

Figure 1. Calibration refinement steps.

The refinement of the calibration is not solely about reducing the re-projected error, as shown in Fig.1, which illustrates the comprehensive process. It initiates from an initial calibration, extracting particle positions from sparse images, typically around $0.005ppp$. The identification of particles in the 3D space can be done by either triangulation or tomographic reconstruction, facilitated by the image's sparsity, aiding in associating sensor and 3D positions. Subsequently, the positions undergo refinement, identifying the poorest-performing particles by assuming a Gaussian error distribution for each $x - y$ direction within the i^{th} camera. Following this, a specific percentage

of the best-performing particles is retained. However, this method presents limitations, notably in a camera affected by localized calibration errors. Here, particles linked to this calibration error zone would be excluded from optimization, impeding any enhancement. To counter this, the employment of K-means clustering (Sculley, 2010) is proposed, aiming for approximately 300-500 particles per cluster to validate the Gaussian distribution. Then, the weakest particles within each cluster can be removed, addressing this issue.

This approach can also be used to expand the validity region (VRE) of the third-order polynomial calibration with some adjustments. Let assume $\mathcal{V}^0 \in [X^0_{min}, X^0_{max}] \times [Y^0_{min}, Y^0_{max}] \times [Z^0_{min}, Z^0_{max}]$ the initial calibration validity region with calibration parameter $A^i_{.,0}$ of the ith camera, I^i a set of images for BA and $\mathcal{V}^{n_s} \in [X^{n_s}_{min}, X^{n_s}_{max}] \times [Y^{n_s}_{min}, Y^{n_s}_{max}] \times [Z^{n_s}_{min}, Z^{n_s}_{max}]$ the target validity region that we want to achieve in n_s number of steps, then following the algorithm 1 a new calibration $A^i_{.,n_s}$ that ensures a validity region $\mathcal{V}^{n_s}$ can be found.

Algorithm 1 Validity Region Expansion (VRE).

Input $\mathcal{V}^0, \mathcal{V}^{n_s}, n_s, A^i_{.,0}, I^i$
$\mathcal{V}^j \leftarrow \mathcal{V}^0$
$A^i_{.,j} \leftarrow A^i_{.,0}$
$dx1 \leftarrow (X^0_{min} - X^{n_s}_{min})/n_s$
$dy1 \leftarrow (Y^0_{min} - Y^{n_s}_{min})/n_s$
$dz1 \leftarrow (Z^0_{min} - Z^{n_s}_{min})/n_s$
$dx2 \leftarrow -(X^0_{max} - X^{n_s}_{max})/n_s$
$dy2 \leftarrow -(Y^0_{max} - Y^{n_s}_{max})/n_s$
$dz2 \leftarrow -(Z^0_{max} - Z^{n_s}_{max})/n_s$
while $j < n_s + 1$ **do**
  $\boldsymbol{X^i} \leftarrow Get\_particle\_position(I^i, A^i_{.,j})$
  $\boldsymbol{X^i} \leftarrow \boldsymbol{X^i} \in \mathcal{V}^j$
  $A^i_{.,j+1} \leftarrow bundle\_adjustment\_refinement(A^i_{.,j}, \boldsymbol{X^i})$
  $\mathcal{V}^{j+1} \in [X^j_{min} - dx1, X^j_{max} + dx2] \times [Y^j_{min} - dy1, Y^j_{max} + dy2] \times [Z^j_{min} - dz1, Z^j_{max} + dz2]$
  $j \leftarrow j + 1$
end while
Output $A^i_{.,n_s}$

3. Test case

The method is tested by applying it to the Tomographic PTV data (Sperotto et al., 2023) of a convection cell with Helium-Filled Soap Bubbles (HFSB). The convection is generated in a tank of size

$60 \times 60 \times 60[cm^3]$ by three resistors providing $15[W]$ of heat. The measurement area is illuminated by $100[mJ]$ pulse from a 5×15 LED array. Four FlowSense FCX 5M-124 cameras are used to do the acquisition, the original sensor size of $5[Mpix]$ is cropped to $1906 \times 1000[pix]$ to achieve a $200[Hz]$ sampling rate. The final measurement volume is $30 \times 16 \times 14[cm^3]$ measure for 3000 time step or $15[s]$.

To examine the capabilities of the VRE, we took the original calibration of the experiment, valid for $[-200, 200] \times [-200, 200] \times [-80, 80]$, and we used it to re-project some synthetic 3D traversing data in $[-80, 80] \times [-50, 50] \times [-35, 35]$. The reprojected points undergo a synthetic Gaussian noising of 1 pixel and then are used to compute a new calibration, in Fig.2 a visualization of the calibration markers is given.

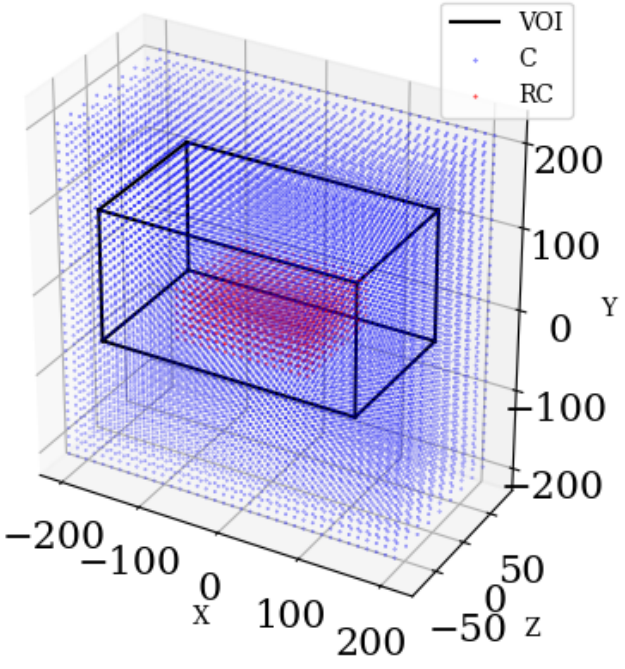

Figure 2. Visualization of: volume of interest (VOI), original calibration markers (C) and the reduced synthetic calibration markers(RC).

A coarse set of ten-time steps with $0.005ppp$ particle density is used for both the VCR, the BA routine and the VRE. In this set of images 33408 particles are seen by all four cameras and the 5% worst particles in any cameras are removed over 66 clusters.

The VRE has been expanded in 5 steps aiming to achieve the final measurement volume. The quality of the final calibration can be assessed qualitatively by comparing the particles identified

in the training data in the first and last steps of the algorithm in Fig.3.

(a) First iteration. (b) Last iteration.

Figure 3. Tracks reconstructed from the training images during the validity region expansion.

The mean re-projection error before and after the BA routine is reported in Table.1. The error is roughly halved for the BA refinement, while the region expansion shows a general improvement except for the last camera. Finally, the BA refinement interpolated particle displacements are

pix	RE 1	RE 2	RE 3	RE 4
Calibration	0.36	0.39	0.34	0.38
BA refinement	0.18	0.20	0.20	0.24
VRE	0.25	0.31	0.28	0.45

Table 1. Reprojection Errors (RE) for the different cameras (1-4)

shown in Fig.4. In the XY plane (Fig.4(a)) the particle displacement is concentrated on the edge and corners especially in lower and upper bound in the $X - axis$. The distribution of the disparity hints that the detection of the point on the edge of the sensor propagates a significant error. In the YZ plane, (Fig.4(b)) a gradient of error from the light centre is present.

The quality of the reconstruction is assessed through two metrics the first one is the Probability Density Function (PDF) of the length of the tracks (Fig.5(a)). Indeed, longer tracks on average are associated with a better reconstruction of the voxel space as ghost particles tend to survive for less time step. The most probable track lengths are 42 (BA), 29 (VRE), 35 (VCR) and 30 for the initial calibration. Similarly, a random particle most likely belongs to a track of length 144 (BA), 108 (VRE), 113 (VCR) and 95 for the initial calibration. The PDFs proposed to take into account tracks and not particles which is why in Fig.5(a) the BA approach seems to have significantly fewer particles than the original calibration even though, this is not the case.

Additionally, the smoothness of the identified particles' position could be an interesting way to assess the quality of the tracks. A good metric for this could be the average jolt energy per track

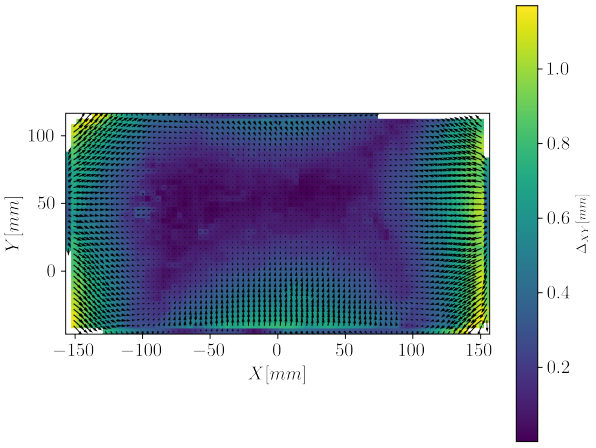

(a) In-plane (XY) particles displacement (Δ_{XY}).

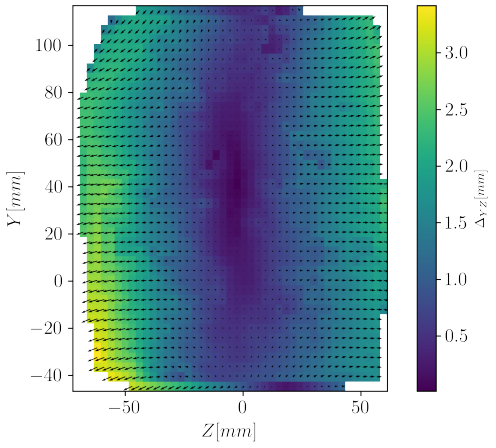

(b) In-plane (YZ) particles displacement (Δ_{YZ}).

Figure 4. In-plane particle displacement.

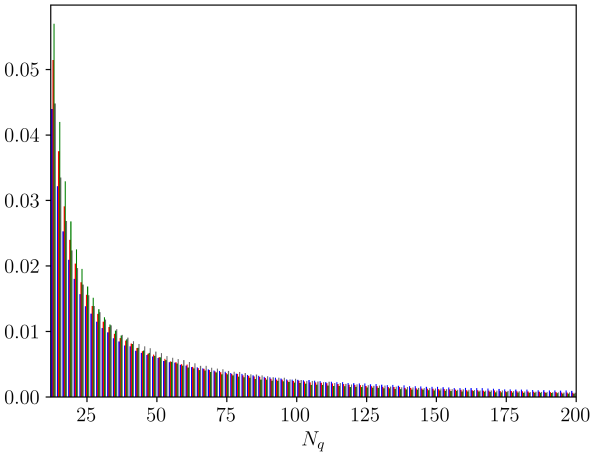

(a) PDF of the lengths of the identified tracks N_q.

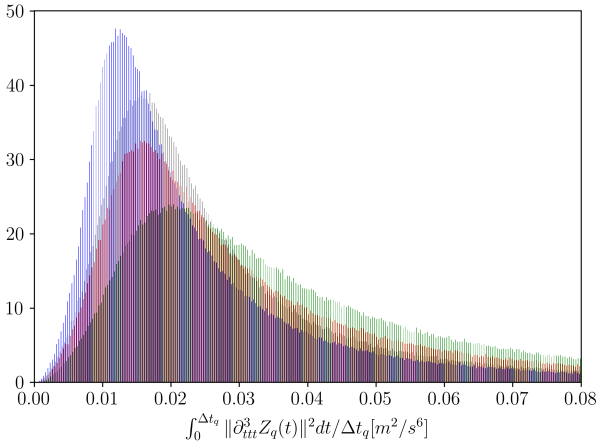

(b) PDF of the average jolt energy in the Z direction per tracks.

Figure 5. PDF for BA (-), VRE (-), VCR (-) and the original calibration (-).

usually a quantity that is desirable to reduce as shown in Gesemann et al. (2016):

$$\frac{1}{\Delta t_q}\int_0^{\Delta t_q} \|\partial^3_{ttt}\boldsymbol{X}_q(t)\|^2 dt, \tag{5}$$

where the subscript q define a quantity associated with the q^{th} track, Δt_q is the existence time of the track and $\boldsymbol{X}_q(t)$ is the trajectory of the particle. In Fig.5(b) the PDF for the average Z jolt energy is shown. The jolt energy shows a clear gradual reduction of the median and a decrease of the standard deviation across the BA, VCR and the original calibration with the BA achieving the best performance. The VRE shows a behaviour in between the classic calibration and the BA.

Finally, the tracks surviving more than 50 snapshots, for both the BA and VCR, are shown in Fig.6. The quantity of tracks seems comparable for both methods except at the corners, where the calibration refinement is not able to retrieve any tracks of meaning. Furthermore, some similarities can be drawn between the correction map Fig.4 and the final tracks. Indeed, the biggest adjustment zones coincide with the increased density of the BA.

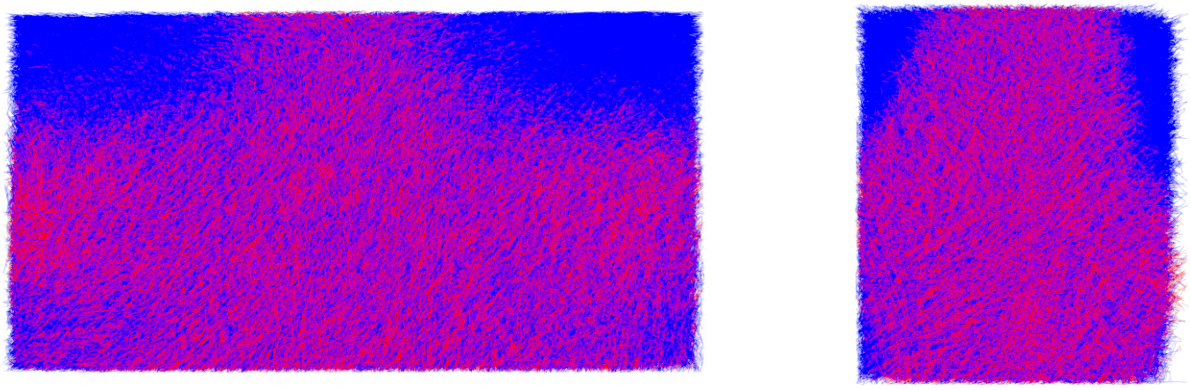

(a) XY view of the particles.

(b) YZ view of the particles.

Figure 6. Views on the final tracked particle; BA in blue and VCR in red.

4. Conclusion

The bundle adjustment showed significantly improved reconstructions with the initial calibration and a good improvement to the VCR. Indeed, as seen in Fig. 4, the improvement seems to be localized at the edges, where the marker detection probably had a higher error in the calibration phase.

The VRE showed a significant result with performance that lays in between the original calibration and the BA refinement. The final goal would to be bring this method to the extreme by using it

with a 2-level target calibration as an initial guess. Tough, still many points must be addressed, for example: the maximum expansion possible, the behaviour of the solution depending on the n_s decided and the behaviour in liquids or with strong density gradients.

References

Bruecker, C., Hess, D., & Watz, B. (2020, March). Volumetric calibration refinement of a multi-camera system based on tomographic reconstruction of particle images. *Optics*, *1*(1), 114–135. Retrieved from http://dx.doi.org/10.3390/opt1010009 doi: 10.3390/opt1010009

Cornic, P., Illoul, C., Le Sant, Y., Cheminet, A., Le Besnerais, G., & Champagnat, F. (2015). Calibration drift within a tomo-piv setup and self-calibration. In *11th international symposium on particle image velocimetry.*

Elsinga, G. E., Scarano, F., Wieneke, B., & van Oudheusden, B. W. (2006, oct). Tomographic particle image velocimetry. *Experiments in Fluids*, *41*(6), 933–947. Retrieved from https://doi.org/10.1007%2Fs00348-006-0212-z doi: 10.1007/s00348-006-0212-z

Gesemann, S., Hunh, F., Schanz, D., & Schröder, A. (2016). From noisy particle tracks to velocity, acceleration and pressure fields using b-splines and penalties. In *Int. symp. on applications of laser techniques to fluid mechanics.*

Maas, H.-G. (1996). Contributions of digital photogrammetry to 3-d ptv. In *Ercoftac series* (p. 191–207). Springer Netherlands. Retrieved from http://dx.doi.org/10.1007/978-94-015-8727-3_9 doi: 10.1007/978-94-015-8727-3_9

Maas, H. G., Gruen, A., & Papantoniou, D. (1993, jul). Particle tracking velocimetry in three-dimensional flows. *Experiments in Fluids*, *15*(2), 133–146. Retrieved from https://doi.org/10.1007%2Fbf00190953 doi: 10.1007/bf00190953

Sculley, D. (2010). Web-scale k-means clustering. In *Proceedings of the 19th international conference on world wide web* (pp. 1177–1178).

Soloff, S. M., Adrian, R. J., & Liu, Z.-C. (1997). Distortion compensation for generalized stereoscopic particle image velocimetry. *Measurement science and technology*, *8*(12), 1441.

Sperotto, P., Petersson, P., Watz, B., & Hess, D. (2023). Instantaneous 3d flow field reconstruction with physics informed radial basis functions. In *15th international symposium on particle image velocimetry – ispiv 2023.* Retrieved from https://scholarworks.calstate.edu/concern/publications/6682xb836

Triggs, B., McLauchlan, P. F., Hartley, R. I., & Fitzgibbon, A. W. (2000). Bundle adjustment — a modern synthesis. In *Lecture notes in computer science* (p. 298–372). Springer Berlin Heidelberg. Retrieved from http://dx.doi.org/10.1007/3-540-44480-7_21 doi: 10.1007/3-540-44480-7_21

Wieneke, B. (2004). Application of self-calibration stereo piv in enclosed measurement volumes. In *Proceedings of the 12th international symposium on the application of laser techniques to fluid mechanics, lisbon, portugal.*

Wieneke, B. (2008, June). Volume self-calibration for 3d particle image velocimetry. *Experiments in Fluids*, *45*(4), 549–556. Retrieved from http://dx.doi.org/10.1007/s00348-008-0521-5 doi: 10.1007/s00348-008-0521-5